Supplementary Information

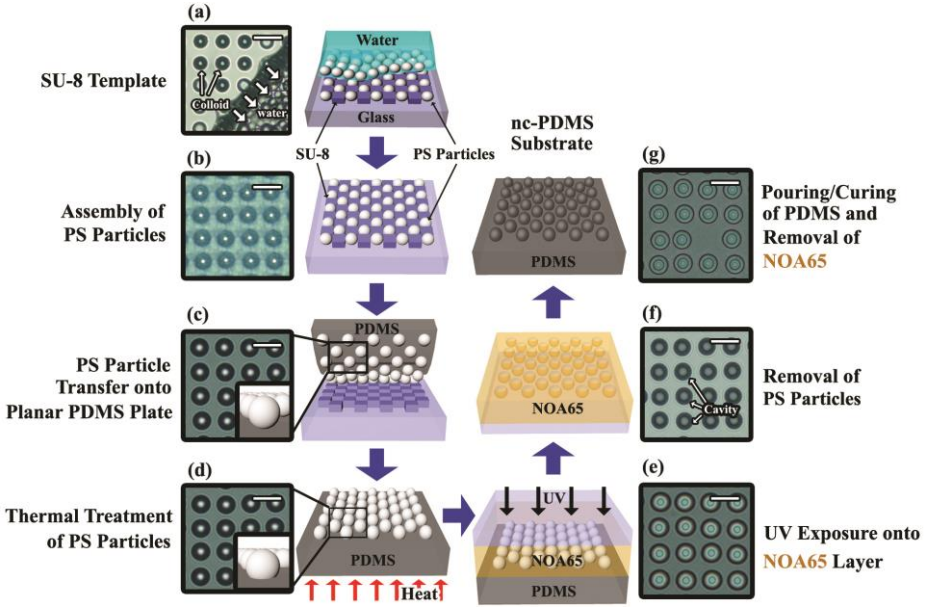

Supplementary Figure 1. Fabrication processes of bud-mimicking PDMS patterns based on a combination of colloidal, soft, and photo-lithography a-d, The polystyrene (PS) particles in colloid were assembled on a periodically patterned SU-8 template through a convective assembly process[1, 2], transferred onto a PDMS plate, and treated thermally for softening and fixation. **e**, A photo-curable polymer (NOA65) layer was coated on the PDMS plate, a glass cover was placed on it, and the whole plate was then exposed to ultraviolet light for 2 min. **f,** After peeling off the PDMS plate, the PS particles were removed from the NOA65 layer in toluene for 1 min. **g**, The PDMS was poured over the NOA65 layer with the PS vacancies and then thermally cured for 3 h. The NOA65 layer was finally removed in a mixed solution for 1 day to leave out only the bud-mimicking patterns of the PDMS (the nc-PDMS substrate).

Note that after the plasma treatment, the nc-PDMS substrate exhibited significant resistance to hydrophobic recovery and stabilized the lipid membranes supported on the PDMS substrate for extended periods of time (up to several days). Scale bars: 50 μm

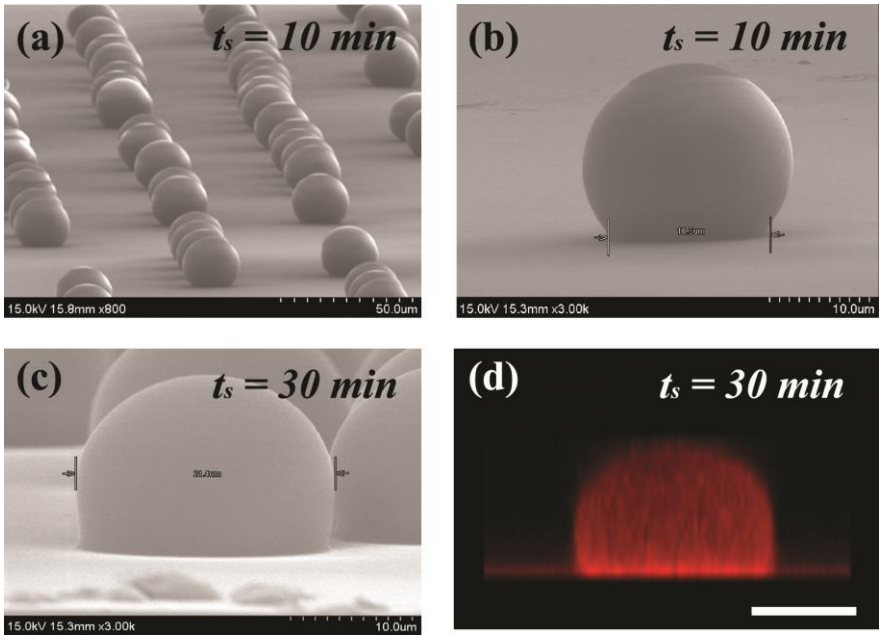

Supplementary Figure 2. The SEM images of the bud-mimicking PDMS patterns and the confocal image (side-view) of the SLB covered on the PDMS pattern a-c, The SEM images of an array (**a**) and one unit (**b**) of the PMDS bud-pits produced at the softening time t_s = 10 min (the bud-neck diameter ≈16 μm). The bud-neck of about 18 μm in diameter was produced at t_s = 30 min (**c**). **d**, The confocal image (side-view) of the SLB covering the PDMS pattern in (**c**). Scale bar: 10 μm

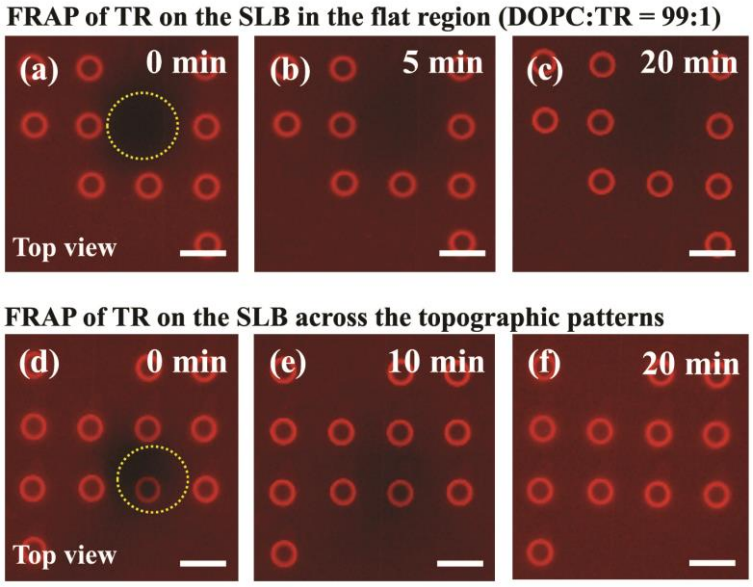

Supplementary Figure 3. Lateral fluidity for the supported B1 membrane (DOPC: TR-DHPE=99:1) in the flat- and the bud-pit regions The fluorescence recovery after photo-bleaching (FRAP)[3] studies were performed at the time of 3 days after the preparation of the SLB. **a-c**, The FRAP results in the flat region at the recovery time of 0, 5, and 20 min. **d-f**, The FRAP results across the topographic patterns with $r \approx$ 100 nm at the recovery time of 0, 10, and 20 min. The yellow dotted circle represents the photo-bleached area. Scale bars: 50 μm

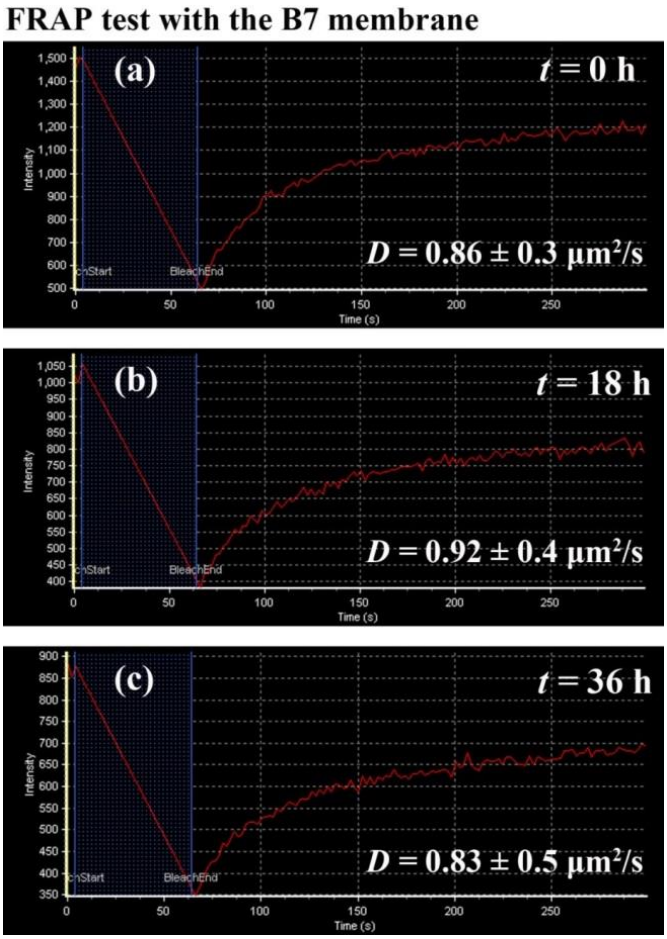

Supplementary Figure 4. Diffusion coefficients in the ring-raft around the collar band at three elapsed times for the B7 membrane (DOPC:SPM:CHOL:TR=33:33:33:1) a-c, The profiles of the fluorescence recovery after photo-bleaching (FRAP) for the B7 membrane supported on the oxidized nc-PDMS substrate at three elapsed times: (a) immediately after vesicle fusion (t = 0 h); (b) 18 hours after vesicle fusion (t = 18 h); and (c) 36 hours after vesicle fusion (t = 36 h). Similar diffusion coefficients over the course of the elapsed time for 36 h ensure the long-term lateral fluidity and the structural contiguity of the SLB.

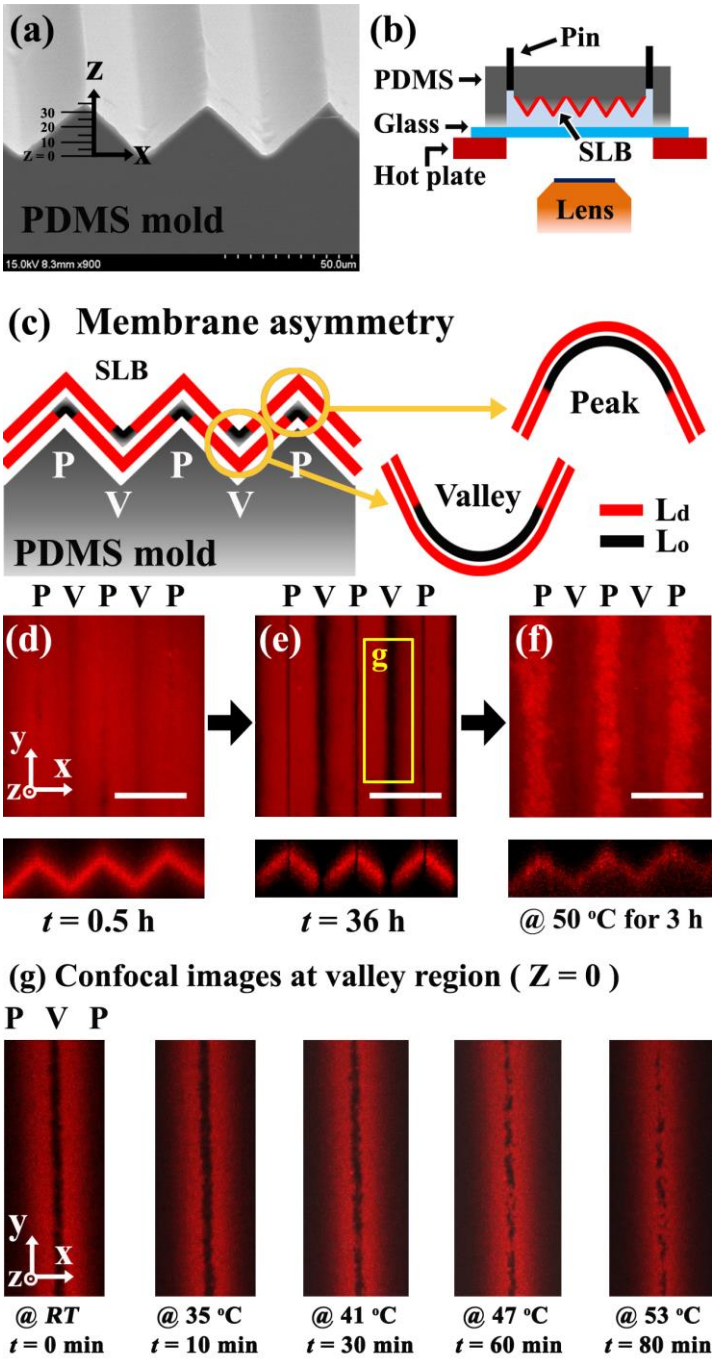

Supplementary Figure 5. Reconstitution of the L_o domains in the prescribed regions with local curvatures and the thermal behavior of topographically structured SLB In determining the thermal behavior of the curvature-driven L_o domain, the PDMS substrate with periodic wedges of the peaks (denoted by P's) and the valleys (denoted by V's) was used as a support for the SLB. The peak-to-peak distance was 50 μm. Note that the wedge substrate represents the essential topographic features of the bud-neck regions and facilitates the observation of the L_o domains without being obscured by the bud-pit. The radius of curvature (r) in the valley or the peak was comparable to that in the bud-neck (r = 100 - 300 nm). The simplicity of the wedge substrate enables to directly characterize the thermal behavior of the L_o domains. **a,** The SEM image of the PDMS substrate with periodic wedges .

b,**c,** Schematic illustration of a custom-designed thermal stage mounted on a confocal fluorescence microscope (b) and reconstitution of the L_o domains in the prescribed regions of local curvatures together with the arrangement of the inner and outer leaflets in the valley and peak regions (c). The inter-leaflet compositional asymmetry may be considered for understanding more delicate interactions but it is beyond the scope of this work. **d,e,** The confocal images projected along the *z*-direction (top) and the cross-sectional images (bottom) obtained for the B7 membrane (DOPC:SPM:CHOL:TR=33:33:33:1) at the duration time of t = 0.5 h (d) and 36 h (e) after vesicle fusion. Clearly, the TR-depleted L_o phase gradually decorated the edges and the raft domain was developed in the valleys and peaks as expected[4]. **f**, Upon heating the SLB sample at 50°C for 3 h, the fluorescence pattern became partially homogenized, indicating that the L_o domains, devoid of fluorescence, were mixed with the surrounding background and lost the preferential localization in the edges. **g**, The thermal and temporal behavior of the raft domain in the valley in the course of heating for 80 min (in a step of 10 min) from room temperature to 53°C. The thermal process of the pattern homogenization and domain dissolution was clearly observed. The images were acquired in a semi-confocal mode where a pinhole was open at the maximum of 800 μm in diameter to obtain a large depth of field per image, allowing to keep the valleys in focus (Z = 0 μm, a yellow rectangular inset depicted in **e**). The observed temperature for the domain dissolution (about 41°C) was found to be somewhat higher than the bulk miscibility transition temperature (38°C). This may be attributed to the error in temperature control in our experimental setup and the effect of the substrate interface[5]. Scale bars: 50 μm

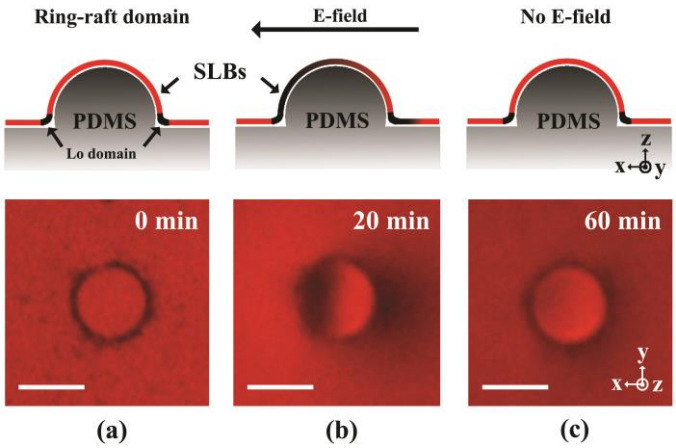

Supplementary Figure 6. The closed ring-raft domain as a barrier to the lipid change between the bud membrane and the donor membrane a-c, The curvature-driven localization of the L_o domain in the SLB was produced before the application of an electric field. The electric field *E* was applied along the *x*-axis from two Pt wires placed 1.5 cm apart. In the bottom, the epifluorescence micrographs observed at t = 0 min (at the time of the application of *E*; **a**), t = 20 min (20 min under E = 45 V/cm; **b**), and t = 60 min (40 min after the removal of *E* at t = 20 min; **c**) were shown. The closed topology of the ring-raft domain indeed serves as a barrier to the lipid exchange across the bud-neck between the bud membrane and the donor membrane. Scale bars: 20 μm

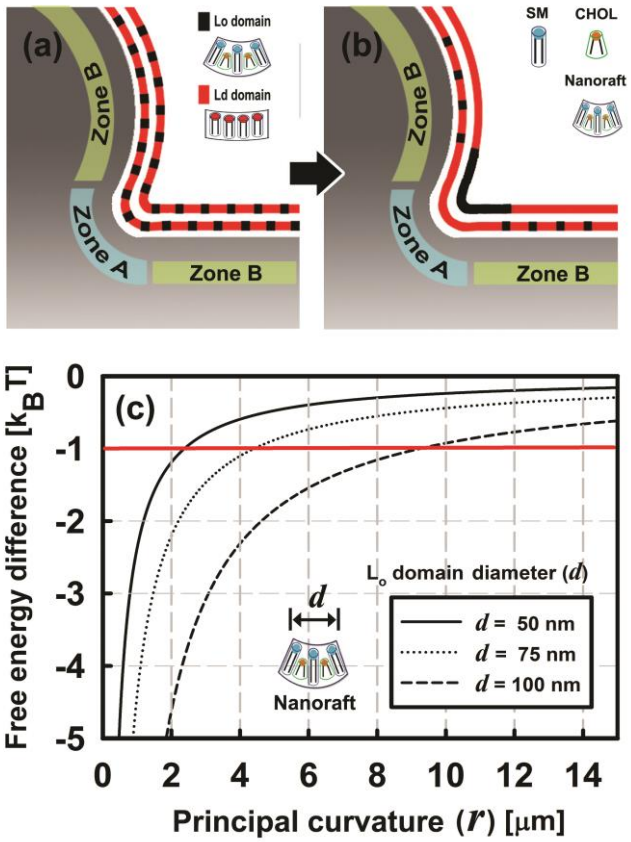

Supplementary Figure 7. A simple model for the preferential coarsening of raft domains at the bud-neck interface The spontaneous curvature of the L_o phase (c_{Lo} = −1/68 Å^{-1})[6], originated from the asymmetry in the lipid molecule[7], has a more negative value than that of the L_d phase (c_{Ld} = −1/160 Å^{-1}) composed of the DOPC molecules[8] (shown in **a**). When the lipid membrane in the bud-neck region (Zone A) is under the structural deformation by the negative curvature of the underlying PDMS substrate, the L_o domain experiences less severe elastic distortions than the L_d domain. In other words, the curvature gradient of the negatively curved membrane provides one of the contributions to the driving force for the accumulation and coarsening of 'nanorafts'[9] at the bud-neck interface. Together with the asymmetric distribution across two monolayer leaflets[10], the curvature gradient leads to the formation of a ring-raft in the outer leaflet around the bud (shown in **b**). More quantitatively[6], two limiting cases for the localization of the L_o domain can be considered within the formalism of the Helfrich-type free energy per unit area[11]; (1) the preferential localization of the L_o phase in Zone A (case I) and (2) the exclusion of the L_o phase from Zone A (case II). In a simple model, the difference in the elastic energy per unit area (Δf) between the two cases as a function of the principle curvature radius (r) can be written as

$$\Delta f = f(\text{case I}) - f(\text{case II})$$

$$= \frac{1}{2}\left(\frac{1}{2}k_{\mathrm{Lo}}(2c_{\text{zone A}} - 2c_{Lo})^2 + \frac{1}{2}k_{\mathrm{Ld}}(2c_{\text{zone B}} - 2c_{\mathrm{Ld}})^2\right)$$
$$- \frac{1}{2}\left(\frac{1}{2}k_{Lo}(2c_{\text{zone B}} - 2c_{Lo})^2 + \frac{1}{2}k_{\mathrm{Ld}}(2c_{\text{zone A}} - 2c_{Ld})^2\right)$$
$$= -\frac{2}{r_{\text{Zone A}}}(k_{\mathrm{Lo}}c_{\mathrm{Lo}} - k_{\mathrm{Ld}}c_{\mathrm{Ld}})$$

$$(\text{ if } c_{\text{zone A}} \ll c_{\mathrm{Lo}},\ c_{\text{zone A}} \ll c_{\mathrm{Ld}},\ c_{\text{zone B}} = 0\ )$$

where $c_{\text{zone B}}$ and $c_{\text{zone A}}$ are the principle curvature in zone B and that in zone A, , respectively, k_{Ld} and k_{Lo} are the bending moduli, and c_{Ld} and c_{Lo} are the spontaneous curvatures. The free energy difference between the two cases is then given by $\Delta f \times \pi(d/2)^2$ where d is the size of the unit raft (or nanoraft).

The free energy differences for three different sizes of the Lo domain were calculated as a function of the principal curvature radius (r) (shown in **c**). The parameters[12-14] used for the calculations were $c_{\mathrm{Ld}} = -1/160$ Å^{-1} $= -62.5$ μm^{-1}, $c_{\mathrm{Lo}} = -1/68$Å^{-1} $= -147.1$ μm^{-1}, $k_{\mathrm{Ld}} = 5\ k_{\mathrm{B}}T$, and $k_{\mathrm{Lo}} = 6.25\ k_{\mathrm{B}}T$. It was found that the coarsening of nanorafts is energetically favored at the bud-neck interface (zone A) in relative to zone B (planar surface) when the free energy difference exceeds thermal energy of 1 $k_{\mathrm{B}}T$ (represented by the red line). For d = 50 nm, the local radius of curvature below $r \leq 2.38$ μm is small enough to accumulate the nanorafts in the bud-neck region. The critical value r was found to increase with increasing d. This might explain the coarsening process of nanorafts to produce a rather wide rim beyond the ring structure. In our case, the curvature radius is in the range of $r \approx 100$ - 900 nm at the bud-neck interface from which the theoretical criterion for the spatial localization of raft units onto a negatively curved surface of the outer leaflet can be made. However, a complete picture of the curvature-based formalism where the interleaflet asymmetry is explicitly taken into account remains to be explored.

Supplementary References

1. Dimitrov, A.S. & Nagayama, K. Continuous convective assembling of fine particles into two-dimensional arrays on solid surfaces. *Langmuir* **12**, 1303-1311 (1996).
2. Bélanger, M.C. & Marois, Y. Hemocompatibility, biocompatibility, inflammatory and in vivo studies of primary reference materials low-density polyethylene and polydimethylsiloxane: A review. *J. Biomed. Mater. Res.* **58**, 467-477 (2001).
3. Yee, C.K., Amweg, M.L. & Parikh, A.N. Membrane photolithography: direct micropatterning and manipulation of fluid phospholipid membranes in the aqueous phase using deep-UV light. *Adv. Mater.* **16**, 1184-1189 (2004).
4. Meinhardt, S., Vink, R.L. & Schmid, F. Monolayer curvature stabilizes nanoscale raft domains in mixed lipid bilayers. *Proc. Nat. Acad. Sci. U.S.A.* **110**, 4476-4481 (2013).
5. Keller, D., Larsen, N.B., Møller, I.M. & Mouritsen, O.G. Decoupled phase transitions and grain-boundary melting in supported phospholipid bilayers. *Phys. rev. lett.* **94**, 025701 (2005).
6. Jeong, C., Lee, S.-W., Yoon, T.-Y. & Lee, S.-D. Water meniscus-directed organization of liquid-ordered domains in lipid monolayer. *J. Nanosci. Nanotech.* **11**, 4527-4531 (2011).
7. Gruner, S.M., Lenk, R.P., Janoff, A.S. & Ostro, N.J. Novel multilayered lipid vesicles: comparison of physical characteristics of multilamellar liposomes and stable plurilamellar vesicles. *Biochem.* **24**, 2833-2842 (1985).
8. Attard, G.S., Templer, R.H., Smith, W.S., Hunt, A.N. & Jackowski, S. Modulation of CTP:phosphocholine cytidylyltransferase by membrane curvature elastic stress. *Proc. Nat. Acad. Sci. U.S.A.* **97**, 9032-9036 (2000).
9. Yoon, T.-Y. *et al.* Topographic control of lipid-raft reconstitution in model membranes. *Nat. Mater.* **5**, 281-285 (2006).
10. Huttner, W.B. & Zimmerberg, J. Implications of lipid microdomains for membrane curvature, budding and fission - Commentary. *Curr. Opin. Cell Biol.* **13**, 478-484 (2001).
11. Safran, S.A. Statistical thermodynamics of surfaces, interfaces, and membranes. (Addison-Wesley Publishing Company, New York; 1994).
12. Crane, J.M. & Tamm, L.K. Role of cholesterol in the formation and nature of lipid rafts in planar and spherical model membranes. *Biophys. J.* **86**, 2965 (2004).
13. Chen, Z. & Rand, R. The influence of cholesterol on phospholipid membrane curvature and bending elasticity. *Biophys. J.* **73**, 267-276 (1997).
14. Collins, M.D. Interleaflet coupling mechanisms in bilayers of lipids and cholesterol. *Biophys. J.* **94**, L32-L34 (2008).